Electron attachment line shapes, cross sections, and rate constants at ultralow energies in CF3SO3H, (CF3SO2)2O, and CF3I

S. H. Alajajian, KF. Man, and A. Chutjian

Citation: The Journal of Chemical Physics **94**, 3629 (1991); doi: 10.1063/1.460687
View online: http://dx.doi.org/10.1063/1.460687
View Table of Contents: http://scitation.aip.org/content/aip/journal/jcp/94/5?ver=pdfcov
Published by the AIP Publishing

Electron attachment line shapes, cross sections, and rate constants at ultralow energies in CF_3SO_3H, $(CF_3SO_2)_2O$, and CF_3I

S. H. Alajajian, K-F. Man, and A. Chutjian
Jet Propulsion Laboratory, California Institute of Technology, Pasadena, California 91109

(Received 17 September 1990; accepted 20 November 1990)

Electron attachment cross sections are reported in the energy range 0–160 meV, and at resolutions of 6.0–6.5 meV (FWHM) for the molecules CF_3SO_3H (triflic acid), $(CF_3SO_2)_2O$ (triflic anhydride), and CF_3I (methyl iodide). Use is made of the Kr photoionization method. Attachment line shapes are deconvoluted from the spectral slit (electron energy) function, and are converted to cross sections by normalization to thermal attachment rate constants at 300 K. Rate constants as a function of mean electron energy are calculated from the cross sections using a Maxwellian electron energy distribution function. Present data are compared with flowing-afterglow, Langmuir-probe (FALP) results in triflic acid and anhydride, and with high-Rydberg ionization results in CF_3I.

I. INTRODUCTION

We report herein electron attachment line shapes, cross sections and rate constants for two of the so-called "superacid" molecules CF_3SO_3H (triflic acid) and $(CF_3SO_2)_2O$ (triflic anhydride), and for CF_3I. As with results in previously reported targets,[1-3] these molecules exhibit abrupt onsets of negative ion formation at zero electron energy. The onsets are a direct consequence of the Wigner threshold law[4] for electron attachment. The attachment proceeds through a neutral–negative ion curve crossing, of appropriate symmetry, at zero energy,[5] and has a dependence with electron energy ϵ varying as $\epsilon^{-1/2}$ for s-wave attachment (or $l=0$, where l is the angular momentum of the captured electron). The molecular curve crossing itself arises because the electron affinity of the dissociating fragment is comparable with the bond dissociation energy of the neutral parent.

From an applications point of view the phenomenon itself, and the molecules which exhibit this s-wave attachment behavior, have interesting use in such areas as threshold electron detection, diffuse-discharge switches, development of negative ion sources, trace detection of drugs and explosives, modification of combustion plasmas, and in monitoring of atmospheric transport and dispersion. Several of these applications have been demonstrated in work from our own laboratory.[6,7]

II. EXPERIMENTAL METHODS

Several experimental techniques have been utilized for measuring attachment cross sections and rate constants in the superacids and CF_3I. Attachment rate constants as a function of temperature have been reported for triflic acid and anhydride using the flowing-afterglow, Langmuir-probe (FALP) method[8] in which the electron density is measured as a function of distance along the flowing afterglow. In CF_3I, the technique of collisional ionization of "nearly free" high-Rydberg atoms has been used[9-11] to measure attachment rates and cross sections at energies below about 25 meV. Thermal attachment rate constants at 300 K in CF_3I have been reported using a pulse radiolysis–microwave cavity method to measure electron density via shifts in the resonance frequency of a cavity.[12]

Present measurements were carried out using the krypton photoionization method described earlier.[1] In this method, one photoionizes the krypton component of a 90% krypton plus 10% target mixture to generate electrons in the energy range 0–200 meV, as determined by the photoionization wavelength. Pressures in the collision region as measured with a capacitance manometer are typically 1.3×10^{-2} Pa for the target gas, and 0.45 Pa for krypton. The resolution in the measurements is determined by the

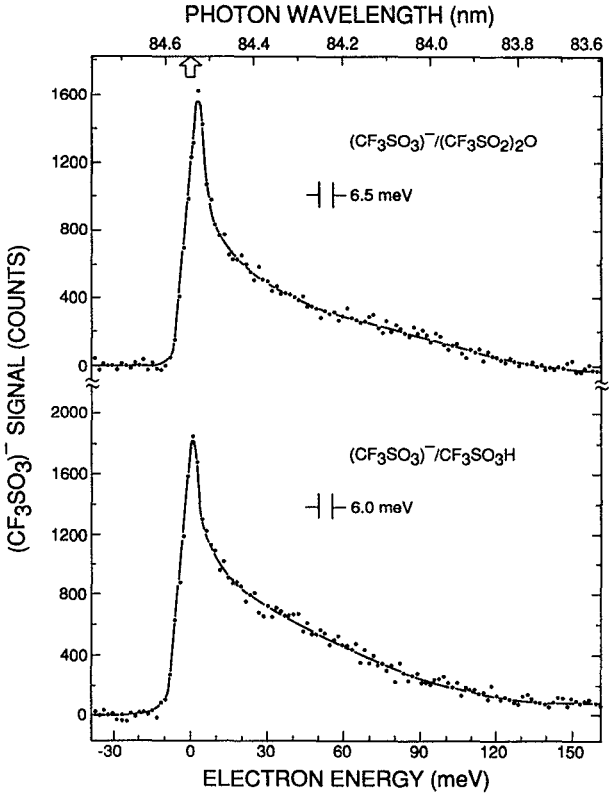

FIG. 1. Attachment line shapes for formation of $CF_3SO_3^-$ from triflic acid (bottom) and triflic anhydride (top) at the indicated resolutions. Full curves are results of computed fits to the experimental data for unfolding. The arrow indicates the threshold at 84.542 nm for ionization to the $^2P_{1/2}$ level of Kr^+.

 0021-9606/91/053629-04$03.00

TABLE I. Summary of cross section parameters a, λ, γ, and N for CF_3SO_3H, $(CF_3SO_2)_2O$, and CF_3I. The attachment cross section is defined by Eq. (1) over the energy range 0–160 meV.

Molecule	$a(eV^{1/2})$	λ(eV)	γ(eV)	$N(cm^2)$	Error in $\sigma_A(\epsilon)$ (%)		$k(\bar{\epsilon})(cm^3/s)$
CF_3SO_3H	6.67×10^{-2}	2.28×10^{-3}	5.60×10^{-2}	1.97×10^{-14}	$\epsilon\leqslant10$ meV	$\epsilon>10$ meV	1.0×10^{-7} [a]
$(CF_3SO_2)_2O$	8.69×10^{-2}	3.44×10^{-3}	6.01×10^{-2}	1.89×10^{-14}	18	15	1.0×10^{-7} [a]
CF_3I	6.98×10^{-2}	2.45×10^{-3}	4.55×10^{-2}	3.81×10^{-14}	18	15	1.7×10^{-7} [b]

[a] Reference 8.
[b] Reference 12.

slitwidth of the vacuum ultraviolet monochromator, assuming negligible broadening by stray electric fields in the collision region. This resolution is typically 5–7 meV (FWHM). The photoelectrons attach to the admixed target in the field-free collision region, and generate a particular negative ion. The ion is extracted, focused, and detected with a quadrupole mass analyzer as a function of the photon wavelength (electron energy).

We report herein attachment lineshapes for the channels $CF_3SO_3^-/CF_3SO_3H$ and $CF_3SO_3^-/(CF_3SO_2)_2O$, shown in Fig. 1; and for the channel I^-/CF_3I. These are the primary channels open at ultralow electron energies, under single-collision conditions (no stabilization with a third body). Experimental conditions of krypton and target pressures, data-accumulation times, and resolution were similar to those of previous studies. In addition, because of the corrosive nature of the superacids, the collision region had to be thoroughly cleaned after their use, and prior to measurements on CF_3I. Before a series of measurements could be started, the apparatus had to be "passivated" with a constant flow of each superacid over a period of several hours. The passivation procedure was monitored by measuring the $CF_3SO_3^-$ signal rate. When the signal rate had stabilized to better than 5%, line shape measurements were initiated. A total of three measurements of the line shape was made for each molecule, and the results averaged. As in previous studies additional measurements were carried out of the high-

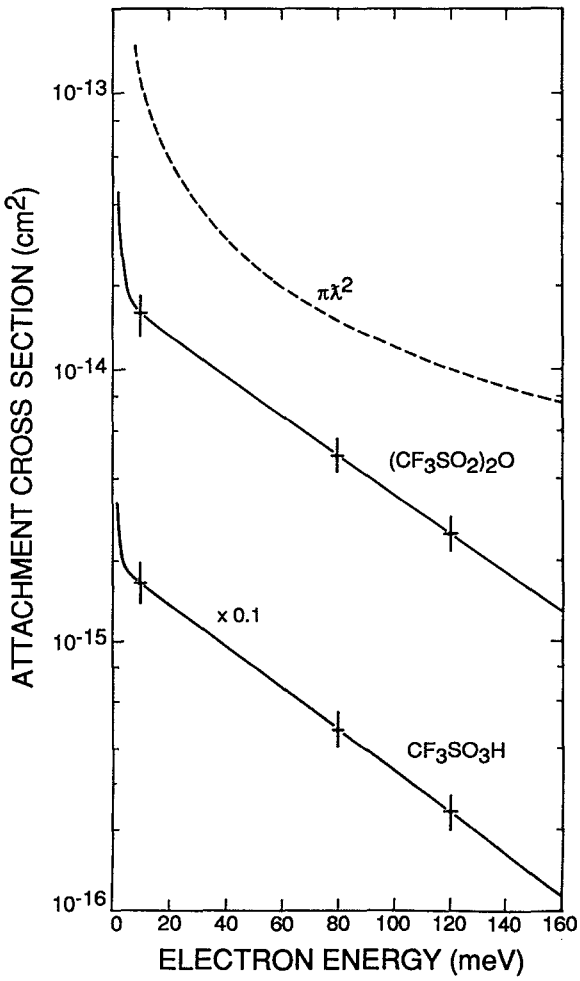

FIG. 2. Cross sections for dissociative electron capture to triflic acid (bottom, multiplied by 0.1) and triflic anhydride (top), with indicated error limits. The maximum s-wave capture cross section $\pi\lambda^{-2}$ (- - -) is shown.

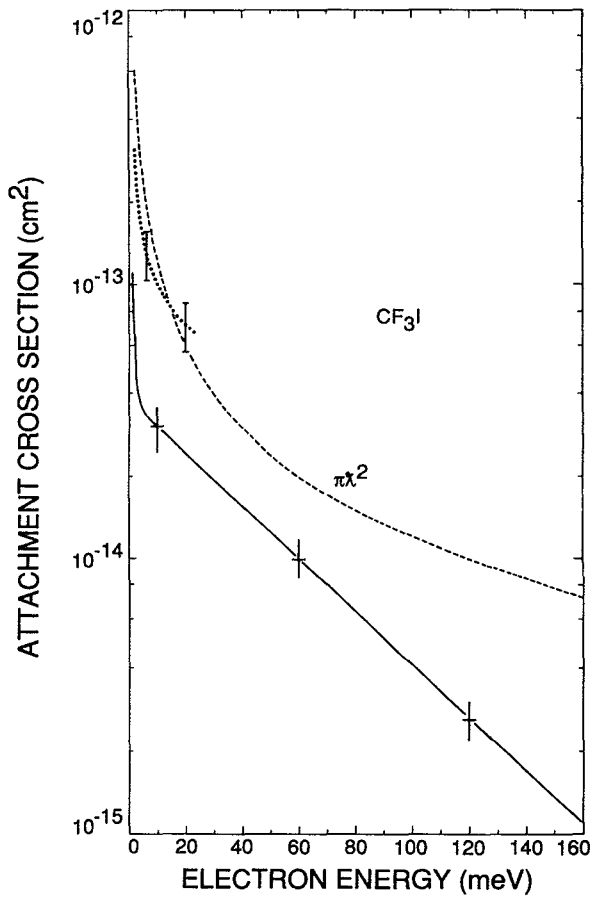

FIG. 3. Cross sections for dissociative electron capture to CF_3I, with indicated error limits. Filled circles (●) are Rydberg ionization results of Ref. 10. The maximum s-wave capture cross section $\pi\lambda^{-2}$(- - -) is shown.

energy ($\epsilon > 10$ meV) slope γ by decreasing the electron energy resolution to about 12 meV. At these higher light levels and hence higher ion count rates, an additional value of γ was obtained for each molecule and averaged with the multichannel scaling values.

The attachment cross section is parametrized in the form

$$\sigma_A(\epsilon) = N[a\epsilon^{-1/2}\exp(-\epsilon^2/\lambda^2) + \exp(-\epsilon/\gamma)], \quad (1)$$

where the parameters a and λ are determined by a computed line fit with the experimental data (Fig. 1), γ from the high-energy ($\epsilon > 10$ meV) portion of the line shape, and N by normalization to the appropriate thermal-attachment rate constant at 300 K through the expression

$$k(\bar{\epsilon}) = (2/m)^{1/2}\int_0^\infty \sigma_A(\epsilon)\epsilon^{1/2}f(\epsilon)d\epsilon, \quad (2)$$

where m is the electron mass, $k(\bar{\epsilon})$ is the thermal attachment rate constant at mean electron energy $\bar{\epsilon} = 38.78$ meV (300 K), and $f(\epsilon)$ is the Maxwellian electron energy distribution function (EEDF) at $\bar{\epsilon}$. The integration in Eq. (2) is carried out numerically.[13]

Implicit in the use of Eq. (2) is the fact that the particular dissociative attachment (DA) channel as measured by $k(\bar{\epsilon})$ (in the FALP or pulse radiolysis experiments[8,12]) and $\sigma_A(\epsilon)$ (present experiments) must be the same. Since the DA channels studied here are the only channels open at these low electron energies, this is the present case. Further discussion of this point can be found in Refs. 1 and 14.

III. RESULTS AND DISCUSSION

Typical results of the computed (deconvolution) fits to the line shape data are shown as solid lines through the experimental points in Fig. 1. Values of a, λ, γ, and N are listed in Table I, along with the values of $k(\bar{\epsilon})$ used to normalize the unfolded line shapes to the cross section scale. Results of the attachment cross sections $\sigma_A(\epsilon)$ for the superacids and CF_3I are shown in Figs. 2 and 3, respectively, along with the maximum s-wave capture cross section defined as $\pi\lambda\!\!\!^{-2}$ (in cm^2) $= 1.197\times10^{-12}\,\epsilon^{-1}$ (ϵ in meV).

Unfortunately, there were no other experimental cross sections with which to compare results in the superacids. However, for CF_3I comparison was possible with recent high-Rydberg collisional ionization cross sections.[10] These results are shown in Fig. 3, and are seen to lie above the present data by a factor of about 3. The reason for this difference is not clear. To see whether the thermal attachment rate constant by which the present data were normalized could be too small by a factor of 3, a separate series of measurements was made of the I^- production signal in CF_3I relative to I^- production in CH_3I. Use was made of the intercomparison technique[15] to measure the ratio of cross sections, a comparison which would reveal any gross errors in measurement of $k(\bar{\epsilon})$. This technique was deemed suitable for the present application, because the mean translational energy imparted to the I^- ions from CH_3I and CF_3I (600 and 820 meV, respectively[11]) were sufficiently close, so that variations in the ion drawout efficiency or lens focusing effects would be small.[3]

Using the intercomparison technique, the ratio of attachment cross sections for the channels I^-/CH_3I and I^-/CF_3I was found to be 1.40 ± 0.09. The ratio was averaged over measurements taken between electron energies of 10 and 40 meV. This ratio compares favorably with the ratio of experimental attachment rate constants of 1.42.[12,16] And hence the reported rate constant in Ref. 12 cannot alone account for the differences in Fig. 3. It is interesting to note that the value of $k(\bar{\epsilon})$ used to normalize the present data [1.7×10^{-7} cm^3/s (Ref. 12)] is considerably smaller than that measured by the Rydberg collisional ionization method [5.9×10^{-7} cm^3/s (Ref. 10)]. Were the latter value used, there would be very good agreement between the two sets of measurements. And hence a possible source of the difference in Fig. 3 could be rate constants for both CF_3I and CH_3I that are too small by a factor of about 3.

Integrations of the cross sections [Eq. (2)] with a Maxwellian EEDF at mean electron energies between 0 and 200 meV yields rate constants, and these are presented in Figs. 4

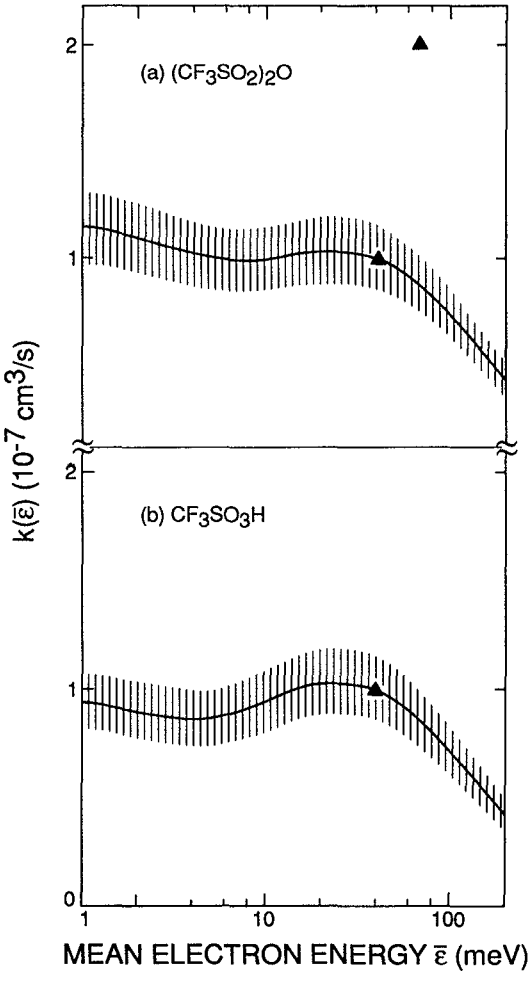

FIG. 4. Attachment rate constants $k(\bar{\epsilon})$ at mean energies $\bar{\epsilon}$ for triflic anhydride (a) and triflic acid (b) with indicated error limits. Filled triangles (▲) are flowing-afterglow, Langmuir-probe (FALP) rate constants of Ref. 8. The effect on the calculated $k(\bar{\epsilon})$ of a changing v,J population of the target with $\bar{\epsilon}$ is taken to be negligible.

and 5. Results in triflic anhydride may be compared with the temperature dependence of $k(\bar{\epsilon})$ as reported in Ref. 8. The latter result at 510 K lies about a factor of 2 above present measurements. This effect, and differences with FALP results, were also noted in results with SF_6.[17] One notes here that the present data reflect results obtained with an electron whose energy is determined by the photoionization wavelength, and a molecule at room temperature. In the FALP results, the molecules are heated to the FALP tube temperature (300 and 510 K). The effect of neglecting the variation of rate constant with a changing v,J population (due to the changing molecular temperature) very likely cannot account for the entire factor-of-two difference. First,the variation given by the FALP results are quite abrupt with temperature; and second, it was shown in earlier work on CCl_4 and $CFCl_3$ (Ref. 5) that the effects of changing v,J could account for only about 20% of the changes in rate constant with T. The major effect arises from the Maxwellian EEDF "sliding up and down" the room-temperature $\sigma_A(\epsilon)$ curves of Fig. 2.

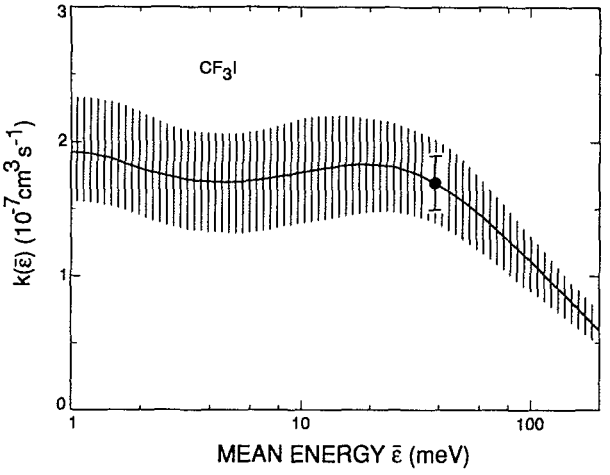

FIG. 5. Attachment rate constant $k(\bar{\epsilon})$ at mean energies $\bar{\epsilon}$ for I^- formation in CF_3I. Filled circle (●) is the measurement of Ref. 12 through which the present cross sections and rate constants are normalized.

Finally, it is interesting to note that the calculated $k(\bar{\epsilon})$ curves in Figs. 4 and 5 approach a constant value as the electron temperature approaches 0 K. Physically, this corresponds to the EEDF narrowing and peaking towards lower energies. At $T < 100$ K, the EEDF samples more of the cross section varying as $\epsilon^{-1/2}$ [Eq.(1)]. And hence the rate constant becomes independent of $\bar{\epsilon}$ [Eq. (2)]—a direct consequence of the Wigner threshold law for attachment at zero energy.

ACKNOWLEDGMENTS

This work was carried out at the Jet Propulsion Laboratory, California Institute of Technology, and was supported by the Department of Energy through agreement with the National Aeronautics and Space Administration.

[1] A. Chutjian and S. H. Alajajian, Phys. Rev. A **31**, 2885 (1985).
[2] A. Chutjian, S. H. Alajajian, and K-F. Man, Phys. Rev. A **41**, 1311 (1990).
[3] S. H. Alajajian, M. T. Bernius, and A. Chutjian, J. Phys. B **21**, 4021 (1988).
[4] E. P. Wigner, Phys. Rev. **73**, 1002 (1948).
[5] O.J. Orient, A. Chutjian, R. W. Crompton, and B. Cheung, Phys. Rev. A **39**, 4494 (1989).
[6] M. T. Bernius and A. Chutjian, J. Appl. Phys. **66**, 2783 (1989); O. J. Orient, A. Chutjian, and S. H. Alajajian, Rev. Sci. Instrum. **56**, 69 (1985).
[7] M. T. Bernius and A. Chutjian, Anal. Chem. **62**, 1345 (1990).
[8] N. G. Adams, D. Smith, A. A. Viggiano, J. F. Paulson, and M. J. Henchman, J. Chem. Phys. **84**, 6728 (1986).
[9] A. Kalamarides, C. W. Walter, B. G. Lindsay, K. A. Smith, and F. B. Dunning, J. Chem. Phys. **91**, 4411 (1989).
[10] Z. Zheng, X. Ling, K. A. Smith, and F. B. Dunning, J. Chem. Phys. **92**, 285 (1990).
[11] C. W. Walter, B. G. Lindsay, K. A. Smith, and F. B. Dunning, J. Chem. Phys. (in press).
[12] H. Shimamori and Y. Nakatani, Chem. Phys. Lett. **150**, 109 (1988).
[13] The integral can also be evaluated in a power series expansion. See the form 3.462-1 in I. S. Gradshteyn and I. M. Ryzhik, *Table of Integrals, Series, and Products* (Academic, New York, 1980). We thank M. Geller for pointing this expansion out to us.
[14] S. M. Spyrou, S. R. Hunter, and L. G. Christophorou, J. Chem. Phys. **83**, 641 (1985); S. R. Hunter and L. G. Christophorou, *ibid.* **80**, 6150 (1984).
[15] S. H. Alajajian and A. Chutjian, J. Phys. B **20**, 2117 (1987).
[16] E. Alge, N. G. Adams, and D. Smith, J. Phys. B **17**, 3827 (1984).
[17] O. J. Orient and A. Chutjian, Phys. Rev. A **34**, 1841 (1986).